ACS OMEGA

http://pubs.acs.org/journal/acsodf

Article

3D Melamine Sponge-Derived Cobalt Nanoparticle-Embedded N-Doped Carbon Nanocages as Efficient Electrocatalysts for the Oxygen Reduction Reaction

Hua Zhang,[▽] Yao Zhou,[▽] Ji Chen, Ziqiu Wang, Zitao Ni, Qianwen Wei, Anran Chen, Meng Li, Tao Sun,* Zhang Jin,* Thomas Wågberg, Guangzhi Hu,* and Xifei Li*

Cite This: *ACS Omega* 2021, 6, 20130−20138

Read Online

ACCESS | Metrics & More | Article Recommendations | Supporting Information

ABSTRACT: The large-scale and controllable synthesis of novel N-doped three-dimensional (3D) carbon nanocage-decorated carbon skeleton sponges (Co-NCMS) is introduced. These Co-NCMS were highly active and durable non-noble metal catalysts for the oxygen reduction reaction (ORR). This hybrid electrocatalyst showed high ORR activity with a diffusion-limiting current of 5.237 mA·cm^{-2} in 0.1 M KOH solution through the highly efficient 4e$^-$ pathway, which was superior to that of the Pt/C catalyst (4.99 mA·cm^{-2}), and the ORR Tafel slope is ca. 67.7 mV·dec^{-1} at a high potential region, close to that of Pt/C. Furthermore, Co-NCMS exhibited good ORR activity in acidic media with an onset potential comparable to that of the Pt/C catalyst. Most importantly, the prepared catalyst showed much higher stability and better methanol tolerance in both alkaline and acidic solutions. The power density obtained in a proton exchange membrane fuel cell was as high as 0.37 W·cm^{-2} at 0.19 V compared with 0.45 W·cm^{-2} at 0.56 V for the Pt/C catalyst. In Co-NCMS, the N-doped carbon nanocages facilitated the diffusion of the reactant, maximizing the exposure of active sites on the surface and protecting the active metallic core from oxidation. This made Co-NCMS one of the best non-noble metal catalysts and potentially offers an alternative approach for the efficient utilization of active transition metals in electrocatalyst applications.

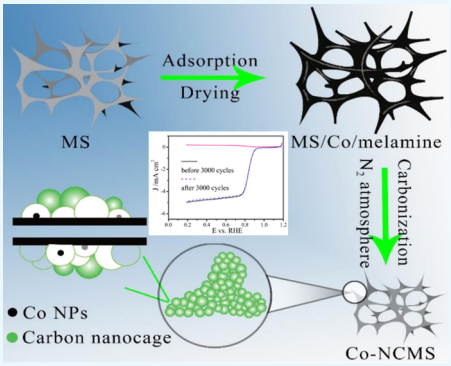

1. INTRODUCTION

The kinetics of the oxygen reduction reaction (ORR) is the key to energy conversion and storage processes in fuel cells, water splitting, oxygen sensors, and metal−air batteries.[1−4] To expedite the ORR and enhance the energy conversion efficiency, an enormous number of effective catalysts are needed. Currently, significant efforts have focused on the development of efficient ORR catalysts using nonprecious metal catalysts, such as Ni, Fe, Co, and their compounds to overcome the scarcity, low stability, and high cost of precious metals.[5−8] However, due to their limitations of low activity, poor durability, and two-electron catalysis process, commercialization opportunities for nonprecious metal-based catalysts are seriously restricted. Therefore, it is necessary to develop alternative ORR catalysts with excellent comprehensive performance to substitute the nonprecious metal-based catalysts.

Many studies have demonstrated that metal−nitrogen−carbon (M−N−C) catalysts have an improved ORR activity and stability in acid and alkaline solution, and even metal-free catalysts based on carbon materials doped by heteroelements (e.g., nitrogen and boron) and metal hydroxides have been used.[9−11] However, these ORR catalysts have a negative onset potential because their catalysis is via a two-electron pathway and is less competitive than Pt/C catalysts in terms of onset potential and reaction current under the same loading amount.[12,13] Additionally, they show limited ORR activity and poor stability in acidic solutions, which makes these catalysts uneconomical for application in a large scale.[14]

According to recent research, metal nanoparticles encapsulated by carbon cages in the microarchitecture (hierarchical meso- and/or macroporosity, etc.) have been developed. Here, the encapsulated metal nanoparticles are crucial in controlling the overall kinetics of the catalysis process, with highly active nanostructures affording good conductivity, reactant accessibility, and high chemical and thermal stability.[15−18] However, resistance defects are inevitable in the carbon framework during the generation of a robust porous architecture. Additionally, it is hard to obtain the desired porosity for highly conductive graphitic carbon and N-doped multidimensional carbon nanomaterials, which significantly limits the conductivity of the ORR process.[2,3,10] Generally, high catalytic

Received: February 25, 2021
Accepted: June 22, 2021
Published: July 27, 2021

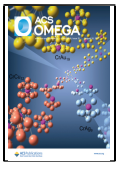

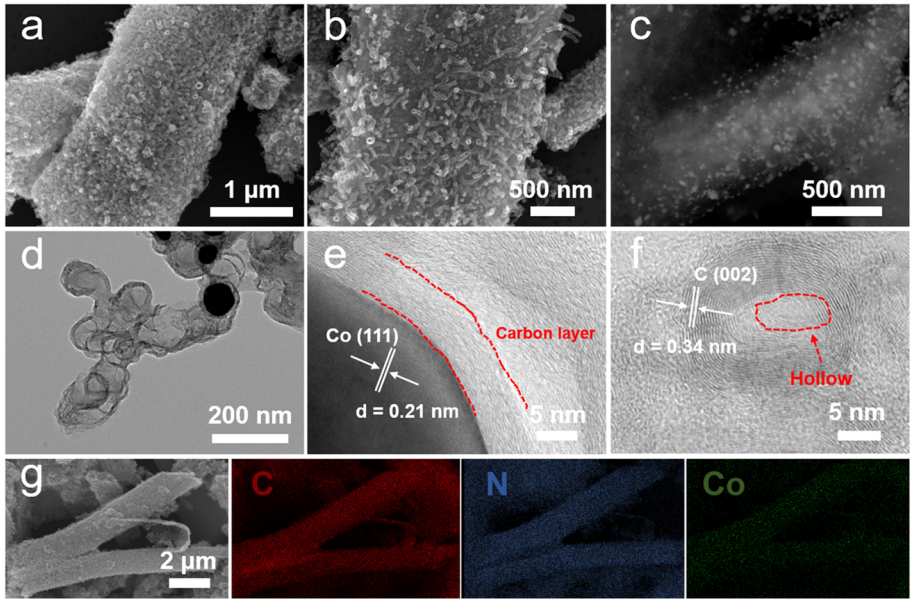

Figure 1. (a, b) Field emission SEM (FESEM) images of the synthesized Co-NCMS catalyst, (c) back-scattered electrons, (d) TEM images, (e, f) HRTEM images, and (g) energy dispersive spectroscopy (EDS) mapping of Co-NCMS.

activity for the ORR has mainly been achieved using Fe−N−C nanocomposites; Co−N−C catalyst is another high-efficiency catalyst, but optimizing the electronic structure of Fe−N−C catalysts to enhance their ORR catalytic activity requires commercially available supports and manageable processing. Therefore, it is highly desirable to develop a method adaptable to large-scale production for synthesizing Co−N−C hybrid catalysts.

In this study, N-doped three-dimensional (3D) carbon nanocage-decorated carbon skeleton sponges (noted as Co-NCMS) were prepared simply by heating melamine sponges (MS) loaded with cobalt particles. The melamine provided the N- and C-containing functional groups of Co-NCMS, which effectively prevented corrosion of the 3D carbon sponges in alkaline or acid medium, and simultaneously solves the problems of excessive defects in the carbon framework by decreasing bulk resistance and inevitable contact resistance from microscopically isolated carbon particles. The combination of the carbon nanocages and the flexible carbon skeleton achieved excellent structural stability. Additionally, the hollow structure of the carbon nanocages was expected to facilitate reactant diffusion in macrospores and maximize the exposure of active sites on the surface.

The prepared Co-NCMS catalyst was effective and durable for the $4e^-$ ORR with high catalytic activity and its performance in the ORR was superior to that of a commercial Pt/C catalyst (20 wt %). The diffusion-limiting current of Co-NCMS was superior to that of Pt/C, and Co-NCMS also exhibited better methanol tolerance than that of Pt/C catalyst in 0.1 M KOH. Furthermore, the carbon nanocages presented good ORR activity in acidic media, comparable to commercial Pt/C catalyst, with a diffusion-limiting current close to that of Pt/C and the $4e^-$ pathway. This strategy provides a novel way to maintain the high activity and stability of nonprecious metals in acidic media and could be further applied in a variety of catalytic systems.

2. RESULTS AND DISCUSSION

In this work, a novel approach is proposed to synthesize the hybrid carbon nanocages grown on 3D hierarchically carbon-doped Co nanoparticles and N atoms via a simple heating strategy. The morphology and structure of the obtained Co-NCMS were characterized by scanning electron microscopy (SEM) and transmission electron microscopy (TEM). Figure 1a,b shows the morphology of Co-NCMS, in which large number of typical nanocages covered the surface of the 3D carbon skeleton. Co-NCMS contained interconnected trestles, like those in bare carbonized MS (prepared by processing MS under the same annealing conditions but without introducing cobalt acetate). Abundant carbon dots were fixed on the surface of the carbonized MS and the porosity of the 3D carbon skeleton from MS remained stable during the calcination process (Figure S1a−c). It is noted that the heating process would cause the collapse in the center of carbon skeleton, produce the hollow structure, and enhance the specific area of Co-NCMS catalysts (Figure S1d); this may be beneficial in providing active sites and absorbing Co ions and subsequently induced the growth of the unique nanocages. The surviving Co nanoparticles were encapsulated into the nanocages and evenly entrapped within the carbon skeleton (Figures 1c and S1e,f), which was surrounded by multishell and Co nanoparticles that were protected in the leaching process by the outer carbon layers.

TEM showed that most of the graphitized nanocages had a hollow structure and diameters within the range of 50−80 nm (Figure 1d) and a wall thickness of only ca. 5 nm (Figure 1f). Most of the graphitization nanocages have a hollow structure and their diameter is statistically measured to be 55.5 ± 9.25 nm (Figure S2), whereas the wall thickness is only ca. 5 nm (see Figure 1e); it is one reason that the obtained Co-NCMS show high Brunauer−Emmett−Teller (BET) surface area. The retained Co nanoparticles were tightly encapsulated in the concentric graphitic carbon shells (dark dots in Figure 1d), which were consistent with the high-resolution TEM (HRTEM) images (Figure 1e). The random graphitic

https://doi.org/10.1021/acsomega.1c01036
ACS Omega 2021, 6, 20130−20138

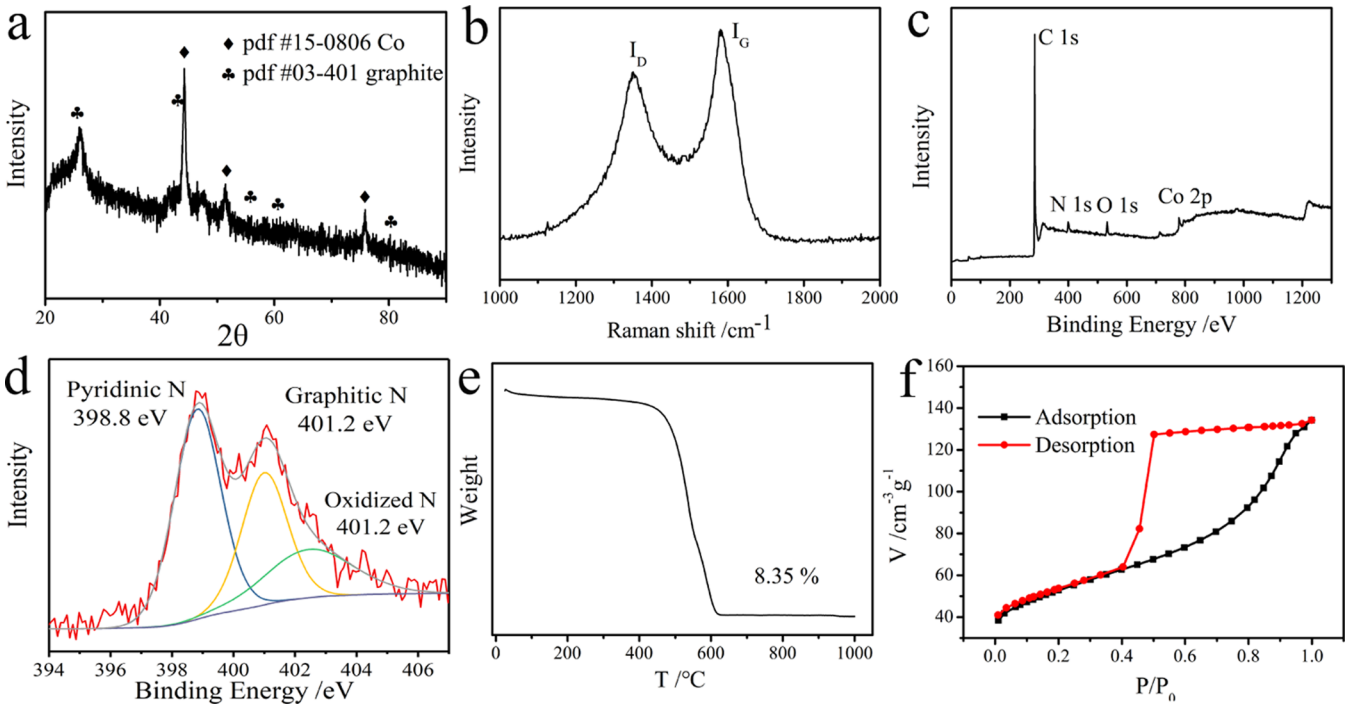

Figure 2. (a) XRD patterns, (b) Raman spectra, (c) X-ray photoelectron spectroscopy (XPS) full spectrum, (d) high-resolution N 1s XPS spectrum, (e) thermogravimetric analysis (TGA), and (f) N_2 adsorption/desorption isotherm curve of the synthesized Co-NCMS catalyst.

nanocage formed a short diffusion channel around the Co-NCMS catalyst and created surface defects by which the adsorption ability of the catalyst was enhanced.

The elemental distribution of a typical Co-NCMS was investigated using field emission scanning electron microscopy (FESEM). As shown in Figure 1g, C (red) and N (blue) are distributed across the whole carbon skeleton surface, while Co (green) is well dispersed in the carbon nanocages and skeleton, further verifying the successful formation of Co-NCMS. The nitrogen doping induced structural defects, which are related to excellent ORR activity.[19,20]

The chemical composition and crystalline structure of the prepared Co-NCMS catalyst were further investigated by applying various techniques. The X-ray diffraction (XRD) pattern corresponded to the typical refraction peaks of metallic cobalt and the sharp peaks suggested that the residual Co nanoparticles had good crystallinity (Figure 2a). A series of XRD peaks revealed the appearance of graphite, with a broad peak at 26° corresponding to the (002) planes of graphitic carbon, mirroring an obvious increase in the crystallinity of melamine as a result of the heating process (Figures 2a and S3).

Raman spectroscopy was also performed to assess the graphitic structure of Co-NCMS and provide information on the disorder and crystallinity of the sp^2-hybridized carbon atoms. As shown in Figure 2b, the ratio of the intensities of the typical D (1348.7 cm^{-1}) and G (1582.3 cm^{-1}) bands, I_D/I_G, is found to be 0.83, revealing that Co-NCMS has a high degree of graphitization with significant defects in the structure.

The pyrolysis temperature and the formation of a carbon cage microstructure play an essential role in the production of active catalytic sites compared to 3D carbon skeleton catalysis materials, and in conjunction with a high defect density lead to improved electrical conductivity.[14,21,22]

X-ray photoelectron spectroscopy (XPS) analysis (Figures 2c and S4a,b) confirmed that Co-NCMS was mainly composed of carbon, nitrogen, oxygen, and cobalt, confirming that N and Co were successfully doped into the 3D carbon skeleton material (Figure S4f). The high-resolution Co spectrum reveals the peaks at 778.31, 780.18, and 794.12 eV (Figure S4b), which are attributed to metallic Co, CoN_x-C_y, and $Co-N_x$ species, respectively; the presence of M−N−C bonds was certified by the existence of CoN_x-C_y and $Co-N_x$ species, which have higher activity toward ORR.[23,24] The presence of oxygen was attributed to oxidation of the carbon material surface when treated under ambient conditions.[25] A high-resolution XPS N 1s spectrum can be deconvoluted into three peaks assignable to the pyridinic (398.7 eV), graphitic (401.9 eV), and oxidized (402.5 eV) nitrogen atoms (Figure 2d) and the nitrogen content as measured is 3.0 atom %.[26,27] The amount of pyridinic N was increased from 14.14% (carbonated MS) to 48.76% with the introduction of carbon nanocages on the 3D carbon skeleton materials (Figure S4c). A high proportion of pyridinic N can increase the current density, spin density, and the density of π states of the C atoms near the Fermi level, thus boosting O_2 reduction.[28−30] The shift of the main peak of XPS spectrum towards lower binding energy was caused by Co doping and the growth of the carbon nanocages (Figure S4d,e). Hence, the high proportion of doped pyridinic N in Co-NCMS probably contributed to its enhanced ORR activity.

Thermogravimetric analysis (TGA) was performed in air with the temperature increasing from 25 to 1000 °C to determine the amount of cobalt in Co-NCMS. As shown in Figure 2e, the amount of Co is calculated to be 6.13% (assuming cobaltous oxide as the ash) and Co-NCMS has a large BET surface area (110.20 m^2·g^{-1}, Figure 2f). Therefore, the goal of generating many defects, O_2 adsorption sites, and, consequently, a high number of active ORR sites was achieved.

https://doi.org/10.1021/acsomega.1c01036
ACS Omega 2021, 6, 20130−20138

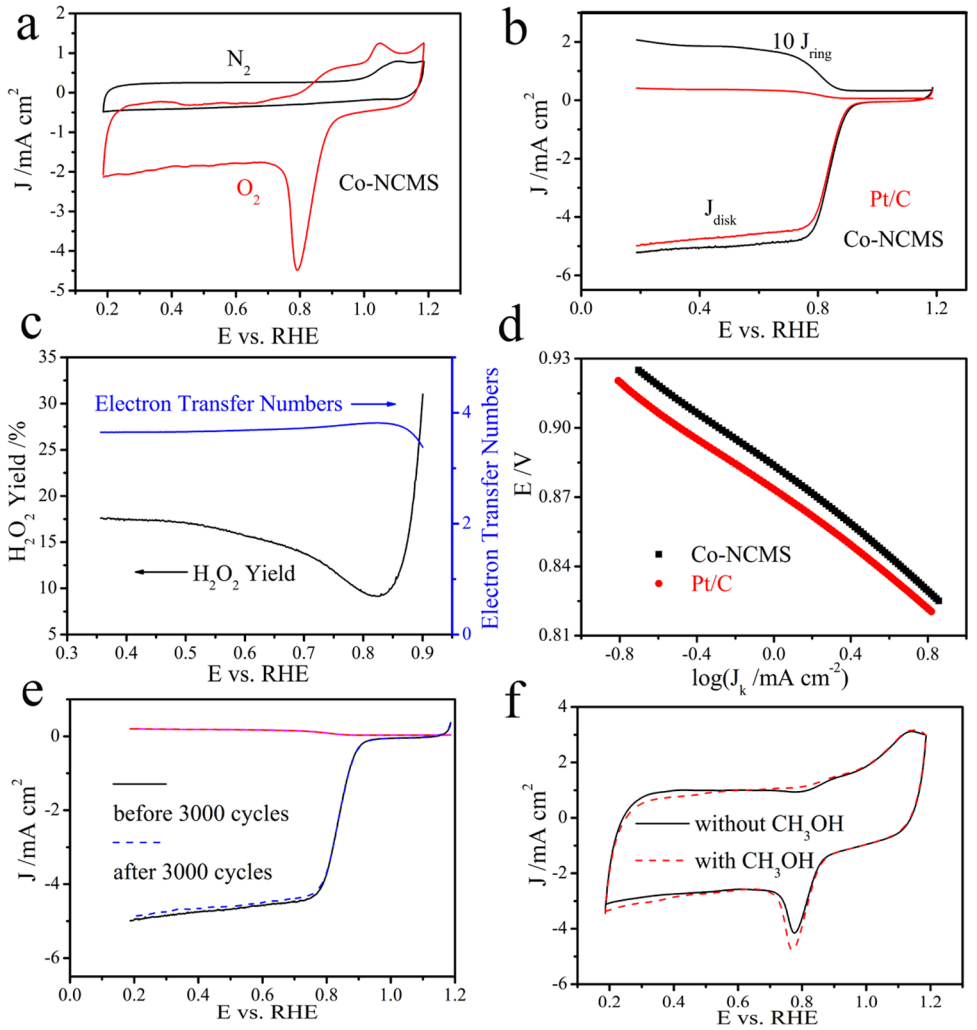

Figure 3. ORR evaluations of Co-NCMS: (a) cyclic voltammetry (CV) curves in O_2- and N_2-saturated 0.1 M KOH solution, (b) RRDE voltammograms, (c) H_2O_2 yield and electron transfer number (n), (d) corresponding Tafel plots obtained from the voltammogram at 1600 rpm in O_2-saturated 0.1 M KOH at a scan rate of 5 mV·s^{-1}, (e) LSV polarization curves for ORR before and after 3000 cycles, and (f) CV curves in O_2-saturated 0.1 M KOH with and without 1.0 M CH_3OH at a scan rate of 50 mV·s^{-1}.

The electrocatalytic activity, stability, and MeOH tolerance of the as-synthesized Co-NCMS catalyst were investigated by the rotating disk electrode (RDE) and rotating ring-disk electrode (RRDE) measurements at room temperature in O_2-saturated 0.1 M KOH solution. For comparison, a commercial Pt/C (20 wt %, the content of Pt is about 4.6 μg) catalyst was also measured under the same conditions (Figure S5). As shown in Figure 3a, there is a distinct reduction in the peak potential centered at 0.791 V for Co-NCMS and a high reaction current of 4.477 mA·cm^{-2}; these results indicated the superior ORR activity of Co-NCMS with a more positive reduction peak potential, onset potential, and higher reduction current density compared to the reported Co-based catalyst (Table S1).[31,32] Remarkably, the Co-NCMS showed a positive onset potential within 11 mV close to that of the Pt/C catalyst value in low overpotential and gave a very sharp current increase (Figure 3b). The polarization curve of Co-NCMS also displayed a diffusion-limiting current beyond that of Pt/C (5.237 vs 4.99 mA·cm^{-2}). Furthermore, the ORR catalytic activity of Co-NCMS was superior to that of commercial Pt/C, as indicated by its more positive (23 mV) half-wave potential ($E_{1/2}$). Most non-noble metal and nonmetal catalysts have weaker catalytic activity and smaller positive ORR onset potentials than those of commercial 20% Pt/C in alkaline media.[33−36] The Co-NCMS catalyst possessed higher ORR catalytic activity compared to Pt/C by giving larger reaction current at low overpotential on the disk, but its ring current was slightly higher.

Koutecky−Levich (K−L) plots were drawn from the RDE polarization curves with various rotation speeds (Figures S6a and 5b). As with the corresponding K−L plots, the data displayed good linearity. The ideal linear relationship between j^{-1} and $\omega^{-1/2}$ can be used to determine the number of electrons transferred (n) based on the Koutecky−Levich equation (Figures S6c). Hence, the 4e$^-$ pathway for reducing O_2 was desirable to acquire maximum energy capacity. RRDE test results (Figure 3c) showed that the H_2O_2 yield obtained with the Co-NCMS catalyst remained below 17% at an overpotential as low as 0.83 V, corresponding to a high electron transfer number of 3.72, close to that of the Pt/C catalyst (n = 3.83, Figures S6d). The high electron transfer number confirmed that most of the O_2 was directly reduced to OH^- without the formation of intermediate peroxides through the highly efficient 4e$^-$ pathway, which was indicative of the extremely high ORR efficiency of the Co-NCMS catalyst.

https://doi.org/10.1021/acsomega.1c01036
ACS Omega 2021, 6, 20130−20138

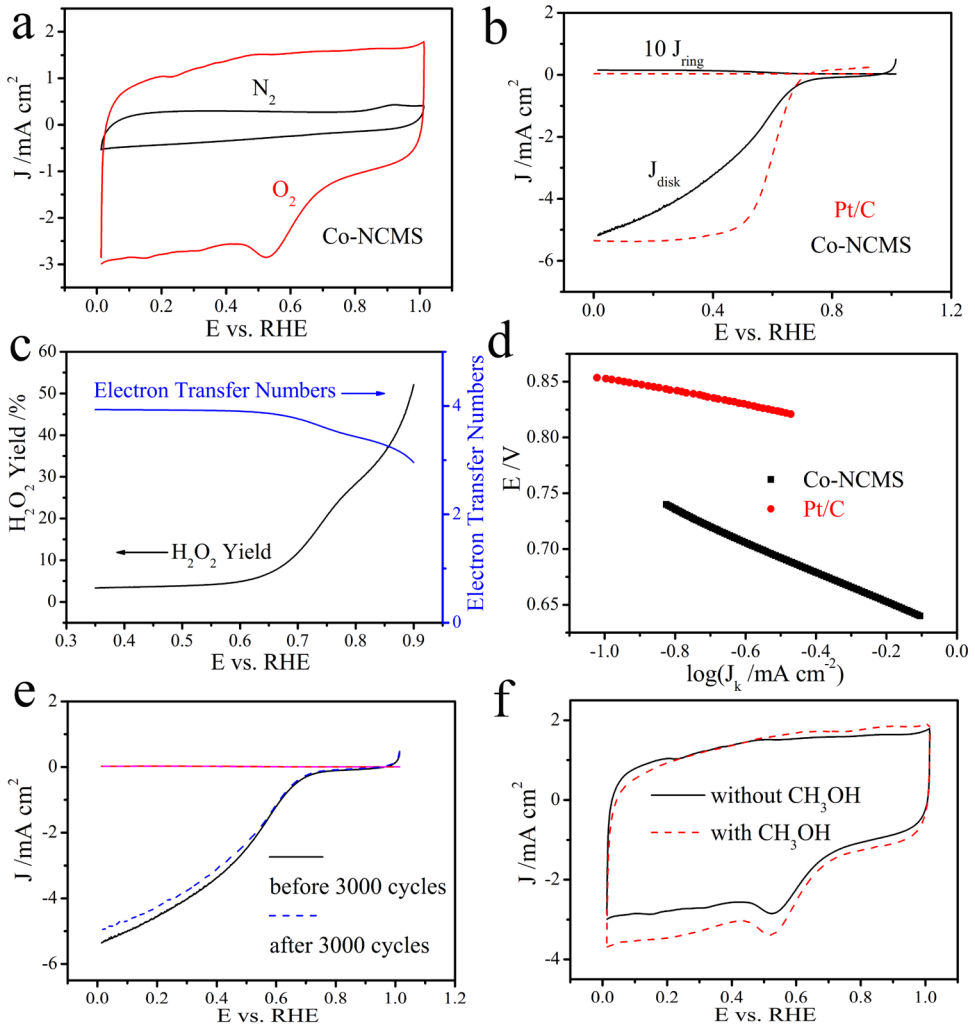

Figure 4. ORR evaluations of Co-NCMS: (a) CV curves in O_2- and N_2-saturated 0.5 M H_2SO_4 solution, (b) RRDE voltammograms (Pt/C in O_2-saturated 0.1 M $HClO_4$), (c) H_2O_2 yield and electron transfer number (n), (d) corresponding Tafel plots obtained from the voltammogram at 1600 rpm in O_2-saturated 0.5 M H_2SO_4 at a scan rate of 5 mV·s^{-1}, (e) linear sweep voltammetry (LSV) polarization curves for ORR before and after 3000 cycles, and (f) CV curves in O_2-saturated 0.5 M H_2SO_4 with and without 1.0 M CH_3OH at a scan rate of 50 mV·s^{-1}.

Figure 3d shows the ORR Tafel slope of the Co-NCMS catalyst is ca. 67.7 mV·dec^{-1} at a high potential region, close to the 64.4 mV·dec^{-1} of the Pt/C. These results indicate that Co-NCMS has an enhanced charge transfer kinetics from the N-doped carbon layer and the Co nanoparticles and an identical ORR mechanism between the carbon nanocage surface and Pt/C catalyst surface.

The stability test of the Co-NCMS catalyst was performed by potential cycling of the catalyst between −0.18 and 1.18 V (vs RHE) in an O_2-saturated 0.1 M KOH solution at a scan rate of 100 mV·s^{-1}. Co-NCMS showed superior durability for ORR in alkaline solution, as confirmed by the absence of an ORR polarization curve shift after 3000 cycles (Figure 3e). Furthermore, to investigate potential poisoning effects on catalytic performance, the tolerance of Co-NCMS against the electrooxidation of methanol (MeOH) was determined by adding 1.0 M MeOH into 0.10 M aqueous KOH. Figure 3f shows almost no change in the ORR peak current for Co-NCMS after addition of MeOH, validating that Co-NCMS has much better methanol tolerance toward ORR. These results were from the structure representation of the Co-NCMS with uniform morphologies, which is probably in favor of improvement of the electrical conductivity. Moreover, the abundant and reasonable pyridinic N atoms and wrinkled surface could also have assumed to provide more defect density and active reaction sites. Accordingly, the enhanced stability and durability can be attributed to Co nanoparticles encased in protective graphitic layers, which diminishes the probability of dissolution of the catalyst.

Interestingly, the Co-NCMS and Pt/C (20 wt %) catalysts were also active and durable for ORR in acidic solution. As shown in Figures 4a and S7, in acidic media there is a distinct reduction peak potential centered at 0.53 V for Co-NCMS with a high reaction current of 2.86 mA·cm^{-2}, which displayed superior ORR activity with a more positive reduction peak potential and a higher reduction current density. The ORR polarization curve of Co-NCMS revealed a high E_{onset} (ca. 0.75 V), close to that of the Pt/C catalyst (0.81 V, Figure 4b) and with a diffusion-limiting current similar to that of Pt/C. The H_2O_2 yield on the Co-NCMS catalyst in acidic solution was more than 10% below 0.7 V (Figure 4c), and the average n value was 3.90, close to the almost constant value of 3.92 for the Pt/C catalyst (Figure S8). Therefore, catalysis of the ORR process by Co-NCMS was mainly through the 4e$^-$ pathway in both alkaline and acidic solution systems.

https://doi.org/10.1021/acsomega.1c01036
ACS Omega 2021, 6, 20130−20138

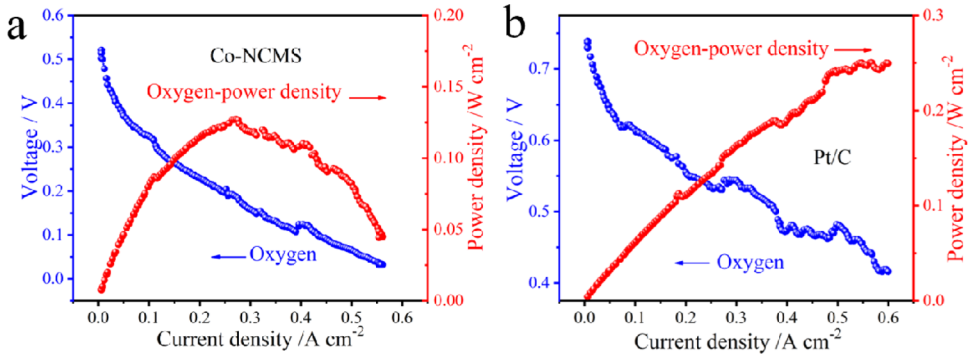

Figure 5. Polarization curves of fuel cells prepared with different catalysts: (a) Co-NCMS at a loading of 5.0 mg·cm^{-2} and (b) Pt/C (20 wt %) at a loading of 0.5 mg·cm^{-2}. The experiments were performed using 30 psi backpressure on both the anode (H_2) and cathode (O_2) compartments, a Nafion115 membrane, and a cell temperature of 80 °C.

The Tafel slope obtained using the Co-NCMS catalyst was 136 mV·dec^{-1} at a low overpotential (Figure 4d), revealing an ideal ability for ORR activity in acidic media, close to that of the Pt/C catalyst (108.5 mV·dec^{-1}).[37−40] The Co-NCMS catalyst also showed much better stability for ORR as revealed by a much lower ORR polarization curve change after 3000 cycles (Figure 4e). This was probably because the protective graphitic layer casing was greatly resistant to acid.

To investigate potential poisoning effects on catalytic performance, the Co-NCMS catalyst was exposed to MeOH to test for a possible crossover effect in the acidic system. In the presence of 1.0 M MeOH, the peak current for Co-NCMS was only slightly changed (Figure 4f), suggesting that Co-NCMS had high selectivity for the ORR and satisfactory tolerance to the crossover effect. The enhanced durability was attributed to the encasing of Co nanoparticles in protective graphitic layers, which diminished the probability of dissolution of the catalyst.

The high percentage of pyridinic N (40.12%) doped into the 3D carbon skeleton resulted in an increased current density, which promoted O_2 adsorption and decreased the local work function of carbon. The carbon nanocages on the Co-NCMS catalyst surface and the hollow structure of the carbon skeleton also enhanced the hydrophilicity of the catalyst and strengthened electrolyte−electrode interactions. Generally, an N dopant-related high structural defect density and the synergistic catalytic effects of the N dopant and carbon-coated Co nanoparticles afford abundant catalytic active sites with a greater turnover frequency. In the present system, the Co nanoparticles and protective graphitic layers, as well as the uniform morphology and structural homogeneity, were thought to account for the enhanced catalytic activity of Co-NCMS towards the ORR because the Co nanoparticles activated the surrounding graphitic layers.

Further, Co-NCMS and commercial Pt/C (20 wt %) were each fabricated into separate membrane−electrode assemblies (MEA) for single-cell performance testing under real operating conditions. The cathode and anode catalyst loadings were 5.0 and 0.5 mg·cm^{-2}, respectively. A relatively high Pt loading was used in this study to ensure that there are no limiting effects of the anode reaction. Initial fuel cell polarization data recorded with Co-NCMS and the commercial Pt/C (20 wt %)-derived cathode catalyst are presented in Figure 5. In good agreement with electrochemical measurements, the open cell voltages of the Co-NCMS and Pt/C cells were 0.53 and 0.74 V, respectively, confirming the higher activity of the Co-NCMS catalyst at high cell voltages to avoid oxygen reduction becoming mass-transport limited. The Co-NCMS catalyst generated 0.27 A·cm^{-2} at 0.19 V and a maximum power density of 0.13 W·cm^{-2}, compared with 0.56 A·cm^{-2} at 0.56 V and a maximum power density of 0.25 W·cm^{-2} for the Pt/C catalyst in the fuel cell test. The difference between the two catalysts may be caused by differences in the nature of the active ORR sites, water tolerance, and/or other factors. However, at high current densities, proton and mass transport become more important. Therefore, unconventional catalyst designs should aim at maximizing the active site density and improving the mass and charge transport.[39,40] As already mentioned, the random graphitic nanocage structure created a short diffusion length around the Co-NCMS catalyst and the hollow structure from the 3D carbon skeleton created surface defects and enhanced mass/charge transport ability. On the other hand, the interactions between the metal and nitrogen atoms embedded in the carbon structure led to the formation of more stable active reaction sites.[41] These results indicated that the Co-NCMS catalyst offers an alternative to stable nonprecious metal catalysts for the ORR in fuel cells.

3. CONCLUSIONS

To sum up, a facile and low-cost strategy for the controlled synthesis of a heterostructured Co-NCMS hybrid catalyst by the simple annealing of a melamine and cobalt acetate mixture was developed in the present work. Large numbers of typical nanocages covered the surface of the 3D carbon skeleton, which was amenable to large-scale production. The Co-NCMS catalyst exhibited excellent ORR activity, higher cycle stability, and better methanol tolerance for ORR in 0.1 M KOH solution than that of the commercially available Pt/C catalyst regarding reaction current density and onset potential. Furthermore, the Co-NCMS catalyst had stable and good ORR catalytic ability in 0.5 M H_2SO_4 solution with a current density close to that of Pt/C. The protective graphitic layers provided acid resistance, making Co-NCMS one of the best-performing nonprecious metal catalysts. The outstanding ORR performance of the Co-NCMS catalyst was due to its uniform morphology, unique carbon nanocage structure, nitrogen doping-related structural defect density, and the synergetic interaction between Co nanoparticles and graphitic layers. Therefore, the synthetic approach in this work not only provides a new protocol for the construction of hybrid carbon nanocages based on 3D hierarchical carbon doping of Co nanoparticles and N-doped catalyst but also offers a new

https://doi.org/10.1021/acsomega.1c01036
ACS Omega 2021, 6, 20130−20138

avenue for the development of low-cost, large-scale, and highly efficient electrocatalysts for energy conversion applications.

4. EXPERIMENTAL SECTION

4.1. Preparation of Co Nanoparticles Encapsulated in NCMS. In a typical procedure of Co-NCMS, MS pieces were washed with ultrapure water and ethanol, and dried at 80 °C overnight. Melamine (0.32 g) and cobalt acetate (0.30 g) were dissolved in 20 mL of methanol under continuous stirring for 30 min to generate a homogeneous solution. Then, 0.5 g MS pieces were immersed into the aforementioned solution and continuously stirred for 30 min to soak with melamine and cobalt acetate. Next, the homogeneous mixture was stirred at 65 °C until methanol was fully evaporated. The dried mixture was placed into a horizontal tube furnace and heated at 600 °C at a rate of 5 °C·min^{-1} and kept at 600 °C for 3 h in N_2 atmosphere. The temperature of the tube furnace was further raised to 800 °C at a rate of 3 °C·min^{-1} and kept at 800 °C for 2 h in the same atmosphere. After the synthesis, the mixture was cooled to ambient temperature and the color of the powder changed from mauve to black. The mixture was then treated with 0.5 M H_2SO_4 for 24 h to remove the redundant Co nanoparticles, and the precipitates were centrifuged and washed with distilled water and ethanol several times, respectively. They were finally redispersed and stored in deionized water. All chemicals were of analytical grade and purchased from Aladdin Industrial Corporation (MS was purchased from Huber Schaumstoffe) and used as-received without further purification.

4.2. Characterization. The morphologies of the synthesized Co-NCMS were observed with an FEI Quanta (FEG 450, energy spectrum: EDAX, Apollo XL-SDD) at an acceleration voltage of 5 kV. TEM analysis was performed on a JEOL JEM-2100 transmission electron microscope operated at an accelerating voltage of 200 kV. XRD patterns were recorded on a Bruker-AXS D8 Advance diffractometer with Cu Kα radiation (λ = 1.5418 Å) and operated at 40 kV voltage and 30 mA current in the range of 15−90°. XPS was obtained with Thermo Fisher Scientific equipped using monochromatic Al Ka radiation (72 W, 12 kV at 1486.6 eV). The binding energies and valence band spectrum were calibrated by referencing the spectra to the C 1s peak for the C−C bond at a binding energy of 284.8 eV. Raman spectra was recorded using a Renishaw 2000 model confocal microscopy Raman spectrometer with an excitation wavelength of 532 nm (Renishaw Ltd., Gloucestershire, U.K.). Thermogravimetric analysis (TGA) was performed with NETZSCH STA 449F3.

4.3. Electrochemical Measurements. The electrochemical measurements were performed with a rotating ring-disk electrode (RRDE) technique in a three-electrode cell at an ambient temperature. An RRDE (Pine Research Instrumentation) was used as the working electrode. The RRDE electrode consisted of a catalyst-coated glassy carbon (GC) disk (with a diameter of 5.61 mm) surrounded by a Pt ring (with inner and outer ring diameters of 6.25 and 7.92 mm, respectively). A platinum net and an Ag/AgCl electrode (saturated with KCl solution) were used as the counter electrode and reference electrode, respectively. More measurement details can be found in the Supporting Information.

■ ASSOCIATED CONTENT

Supporting Information

The Supporting Information is available free of charge at https://pubs.acs.org/doi/10.1021/acsomega.1c01036.

Electrochemical measurements; performance tests of membrane−electrode assemblies; FESEM images and magnifying SEM images; particle size distribution of the graphitized nanocages; XRD patterns and XPS spectrum; CV curves and RDE voltammograms; and ORR performances of Co-NCMS and other reported electrocatalyst (PDF)

■ AUTHOR INFORMATION

Corresponding Authors

Tao Sun − *School of Materials and Energy, Yunnan University, Kunming 650091, P. R. China*; Phone: +86-871-650-31829; Email: t.sun@griffith.edu.au

Zhang Jin − *School of Materials and Energy, Yunnan University, Kunming 650091, P. R. China*; Phone: +86-871-650-31829; Email: 380235683@qq.com

Guangzhi Hu − *School of Materials and Energy, Yunnan University, Kunming 650091, P. R. China; College of Chemistry and Molecular Engineering, Zhengzhou University, Zhengzhou 450000, P. R. China;* orcid.org/0000-0003-0324-2788; Email: guangzhihu@ynu.edu.cn

Xifei Li − *Xi'an Key Laboratory of New Energy Materials and Devices, Institute of Advanced Electrochemical Energy & School of Materials Science and Engineering, Xi'an University of Technology, Xi'an 710048, China;* orcid.org/0000-0002-4828-4183; Phone: +86-29-82312994; Email: xfli2011@hotmail.com

Authors

Hua Zhang − *School of Materials and Energy, Yunnan University, Kunming 650091, P. R. China*

Yao Zhou − *School of engineering, University of Edinburgh, Edinburgh EH9 3JW, England*

Ji Chen − *School of Materials and Energy, Yunnan University, Kunming 650091, P. R. China*

Ziqiu Wang − *MOE Key Laboratory of Macromolecular Synthesis and Functionalization, Department of Polymer Science and Engineering, Key Laboratory of Adsorption and Separation Materials & Technologies of Zhejiang Province, Zhejiang University, Hangzhou 310027, P. R. China*

Zitao Ni − *School of Materials and Energy, Yunnan University, Kunming 650091, P. R. China*

Qianwen Wei − *School of Materials and Energy, Yunnan University, Kunming 650091, P. R. China*

Anran Chen − *School of Materials and Energy, Yunnan University, Kunming 650091, P. R. China*

Meng Li − *College of Chemistry and Molecular Engineering, Zhengzhou University, Zhengzhou 450000, P. R. China*

Thomas Wågberg − *Department of Physics, Umeå University, SE-90187 Umeå, Sweden;* orcid.org/0000-0002-5080-8273

Complete contact information is available at: https://pubs.acs.org/10.1021/acsomega.1c01036

Author Contributions

$^{\nabla}$H.Z. and Y.Z. contributed equally.

Notes

The authors declare no competing financial interest.

https://doi.org/10.1021/acsomega.1c01036
ACS Omega 2021, 6, 20130−20138

■ ACKNOWLEDGMENTS

This work was financially supported by the National Key R&D Program of China (2019YFC1804400), the National Natural Science Foundation of China (21677171, 21505154, and 51621001), the Double Tops Joint Fund of the Yunnan Science and Technology Bureau and Yunnan University (2019FY003025), the East-Land Middle-aged and Young Backbone Teacher of Yunnan University (No. C176220200), and Yunnan Applied Basic Research Projects (202001BB050006 and 202001BB050007).

■ REFERENCES

(1) Li, Y.; Liu, D.; Gan, J.; Duan, X.; Zang, K.; Ronning, M.; Song, L. Sustainable and Atomically Dispersed Iron Electrocatalysts Derived from Nitrogen- and Phosphorus-Modified Woody Biomass for Efficient Oxygen Reduction. *Adv. Mater. Interfaces* **2018**, *6*, No. 1801623.

(2) Seh, Z. W.; Jakob, K.; Colin, F. D.; Ib, C.; Jens, K. N.; Thomas, F. J. Combining theory and experiment in electrocatalysis: Insights into materials design. *Science* **2017**, *355*, No. eaad4998.

(3) Zhang, J.; Yufei, Z.; Xin, G.; Chen, C.; Chung, L. D.; Ru, S. L.; Chih, P. H.; Yadong, L.; Yury, G.; Guoxiu, W. Single platinum atoms immobilized on an MXene as an efficient catalyst for the hydrogen evolution reaction. *Nat. Catal.* **2018**, *1*, 985−992.

(4) Li, M.; Liu, T.; Bo, X.; Zhou, M.; Guo, L.; Guo, S. Hybrid carbon nanowire networks with Fe-P bond active site for efficient oxygen/hydrogen-based electrocatalysis. *Nano Energy* **2017**, *33*, 221−228.

(5) Strickland, K.; Ryan, P.; Elise, M.; Qingying, J.; Ivo, Z.; Shraboni, G.; Wentao, L.; Sanjeev, M. Anion Resistant Oxygen Reduction Electrocatalyst in Phosphoric Acid Fuel Cell. *ACS Catal.* **2018**, *8*, 3833−3843.

(6) Choi, C. H.; Claudio, B.; Jan, P. G.; Anna, K. S.; Frederic, J.; Karl, J. J. M. Stability of Fe-N-C Catalysts in Acidic Medium Studied by Operando Spectroscopy. *Angew. Chem., Int. Ed.* **2015**, *54*, 12753−12757.

(7) Zhu, C.; Qiurong, S.; Bo, Z. X.; Shaofang, F.; Gang, W.; Ce, Y.; Siyu, Y.; Junhua, S.; Hua, Z.; Dan, D.; Scott, P. B.; Dong, S.; Yuehe, L. Hierarchically Porous M-N-C (M = Co and Fe) Single-Atom Electrocatalysts with Robust MN_x Active Moieties Enable Enhanced ORR Performance. *Adv. Energy Mater.* **2018**, *8*, No. 1801956.

(8) Gong, M.; Yanguang, L.; Hailiang, W.; Yongye, L.; Justin, Z. W.; Jigang, Z.; Jian, W.; Tom, R.; Fei, W.; Hongjie, D. An Advanced Ni-Fe Layered Double Hydroxide Electrocatalyst for Water Oxidation. *J. Am. Chem. Soc.* **2013**, *135*, 8452−8455.

(9) Liang, J.; Rui, F. Z.; Xue, M. C.; You, H. T.; Shi, Z. Q. Fe-N Decorated Hybrids of CNTs Grown on Hierarchically Porous Carbon for High-Performance Oxygen Reduction. *Adv. Mater.* **2014**, *26*, 6074−6079.

(10) Lu, X.; Wai, L. Y.; Bryan, H. R. S.; Chuan, Z. Electrocatalytic Oxygen Evolution at Surface-Oxidized Multiwall Carbon Nanotubes. *J. Am. Chem. Soc.* **2015**, *137*, 2901−2907.

(11) Li, J.; Mengjie, C.; David, A. C.; Sooyeon, H.; Maoyu, W.; Boyang, L.; Kexi, L.; Stavros, K.; Marcos, L.; Hanguang, Z.; Chao, L.; Hui, X.; George, E. S.; Zhenxing, F.; Dong, S.; Karren, L. M.; Guofeng, W.; Zhenbo, W.; Gang, W. Atomically dispersed manganese catalysts for oxygen reduction in proton-exchange membrane fuel cells. *Nat. Catal.* **2018**, *1*, 935−945.

(12) Wen, Z.; Suqin, C.; Fei, Z.; Xinliang, F.; Shumao, C.; Shun, M.; Shenglian, L.; Zhen, H.; Junhong, C. Nitrogen-Enriched Core-Shell Structured Fe/Fe_3C-C Nanorods as Advanced Electrocatalysts for Oxygen Reduction Reaction. *Adv. Mater.* **2012**, *24*, 1399−1404.

(13) Yang, W.; Xiangjian, L.; Xiaoyu, Y.; Jianbo, J.; Shaojun, G. Bamboo-like Carbon Nanotube/Fe_3C Nanoparticle Hybrids and Their Highly Efficient Catalysis for Oxygen Reduction. *J. Am. Chem. Soc.* **2015**, *137*, 1436−1439.

(14) Zhang, Z.; Junting, S.; Feng, W.; Liming, D. Efficient Oxygen Reduction Reaction (ORR) Catalysts Based on Single Iron Atoms Dispersed on aHierarchically Structured Porous Carbon Framework. *Angew. Chem., Int. Ed.* **2018**, *57*, 9038−9043.

(15) Gao, Y.; Zhewei, C.; Xingchen, W.; Zhilie, L.; Ping, W.; Chenxin, C. Graphdiyne-Supported Single-Atom-Sized Fe Catalysts for the Oxygen Reduction Reaction: DFT Predictions and Experimental Validations. *ACS Catal.* **2018**, *8*, 10364−10374.

(16) Tavakkoli, M.; Tanja, K.; Olivier, R.; Albert, G. N.; Christoffer, J.; Jani, S.; Hua, J.; Esko, I. K.; Kari, L. Single-Shell Carbon-Encapsulated Iron Nanoparticles: Synthesis and High Electrocatalytic Activity for Hydrogen Evolution Reaction. *Angew. Chem., Int. Ed.* **2015**, *54*, 4535−4538.

(17) Deng, J.; Pengju, R.; Dehui, D.; Xinhe, B. Enhanced Electron Penetration through an Ultrathin Graphene Layer for Highly Efficient Catalysis of the Hydrogen Evolution Reaction. *Angew. Chem., Int. Ed.* **2015**, *54*, 2100−2104.

(18) Yang, Y.; Kaitian, M.; Shiqi, G.; Hao, H.; Guoliang, X.; Zhiyu, L.; Peng, J.; Changlai, W.; Hui, W.; Qianwang, C. O-, N-Atoms-Coordinated Mn Cofactors within a Graphene Framework as Bioinspired Oxygen Reduction Reaction Electrocatalysts. *Adv. Mater.* **2018**, *30*, No. 1801732.

(19) Hu, C.; Liming, D. Doping of Carbon Materials for Metal-Free Electrocatalysis. *Adv. Mater.* **2019**, *31*, No. 1804672.

(20) Wang, J.; Yu, C. K. C. W.; Jun, W. In Situ Three-Dimensional Synchrotron X-Ray Nanotomography of the (De)lithiation Processes in Tin Anodes. *Angew. Chem., Int. Ed.* **2014**, *53*, 4460−4464.

(21) Zou, X.; Xiaoxi, H.; Anandarup, G.; Rafael, S.; Bhaskar, R. S.; Eliska, M.; Tewodros, A. Cobalt-Embedded Nitrogen-Rich Carbon Nanotubes Efficiently Catalyze Hydrogen Evolution Reaction at All pH Values. *Angew. Chem., Int. Ed.* **2014**, *53*, 4372−4376.

(22) Qian, Y.; Pan, D.; Ping, W.; Chenxin, C.; Dominic, F. G. Chemical Nature of Catalytic Active Sites for the Oxygen Reduction Reaction on Nitrogen-Doped Carbon-Supported Non-Noble Metal Catalysts. *J. Phys. Chem. C* **2016**, *120*, 9884−9896.

(23) Peera, S. G.; Jayaraman, B.; Nam, H. K.; Joong, H. L. Sustainable Synthesis of Co@NC Core Shell Nanostructures from Metal Organic Frameworks via Mechanochemical Coordination Self-Assembly: An Efficient Electrocatalyst for Oxygen Reduction Reaction. *Small* **2018**, *14*, No. 1800441.

(24) Rui, T.; Guo, P. L.; Xin, Z.; Xun, C.; Zhong, C. The synergistic catalysis on Co nanoparticles and CoNx sites of aniline-modified ZIF derived Co@NCs for oxidative esterification of HMF. *Chin. Chem. Lett.* **2021**, *32*, 685−690.

(25) Gong, K.; Feng, D.; Zhenhai, X.; Michael, D.; Liming, D. Nitrogen-Doped Carbon Nanotube Arrays with High Electrocatalytic Activity for Oxygen Reduction Kuanping. *Science* **2009**, *323*, 760−764.

(26) Wendu, Z.; Jiawei, Q.; Peiyao, B.; Huifen, W.; Lang, X. High-level nitrogen-doped, micro/mesoporous carbon as an efficient metal-free electrocatalyst for the oxygen reduction reaction: optimizing the reaction surface area by a solvent-free mechanochemical method. *New J. Chem.* **2019**, *43*, 10878−10886.

(27) Bai, P.; Weiqi, L.; Chuang, C. Y.; Shi, I. W.; Lang, X. Boosting electrochemical performance of activated carbon by tuning effective pores and synergistic effects of active species. *J. Colloid Interface Sci.* **2021**, *587*, 290−301.

(28) Liang, J.; Yan, J.; Mietek, J.; Shi, Z. Q. Sulfur and Nitrogen Dual-Doped Mesoporous Graphene Electrocatalyst for Oxygen Reduction with Synergistically Enhanced Performance. *Angew. Chem., Int. Ed.* **2012**, *51*, 11496−11500.

(29) Daems, N.; Sheng, X.; Vankelecom, I. F. J.; Pescarmona, P. P.Pescarmona, Metal-free doped carbon materials as electrocatalysts for the oxygen reduction reaction. *J. Mater. Chem. A* **2014**, *2*, 4085−4110.

(30) Cao, T.; Dingsheng, W.; Jiatao, Z.; Chuanbao, C.; Yadong, L. Bamboo-Like Nitrogen-Doped Carbon Nanotubes with Co Nanoparticles Encapsulated at the Tips: Uniformand Large-Scale Synthesis

https://doi.org/10.1021/acsomega.1c01036
ACS Omega 2021, 6, 20130−20138

and High-Performance Electrocatalysts for Oxygen Reduction. *Chem. - Eur. J.* **2015**, *21*, 14022−14029.
(31) Wang, S.; Lipeng, Z.; Zhenhai, X.; Ajit, R.; Dong, W. C.; Jong, B. B.; Liming, D. BCN Graphene as Efficient Metal-Free Electrocatalyst for the Oxygen Reduction Reaction. *Angew. Chem., Int. Ed.* **2012**, *51*, 4209−4212.
(32) Zheng, Y.; Yan, J.; Lei, G.; Mietek, J.; Shi, Z. Q. Two-Step Boron and Nitrogen Doping in Graphene for Enhanced Synergistic Catalysis. *Angew. Chem., Int. Ed.* **2013**, *52*, 3110−3116.
(33) Zheng, B.; Jiong, W.; Feng, B. W.; Xing, H. X. Low-loading cobalt coupled with nitrogen-doped porous graphene as excellent electrocatalyst for oxygen reduction reaction. *J. Mater. Chem. A* **2014**, *2*, 9079−9084.
(34) Zhang, S.; Heyou, Z.; Qing, L.; Shengli, C. Fe−N doped carbon nanotube/graphene composite: facile synthesis and superior electrocatalytic activity. *J. Mater. Chem. A* **2013**, *1*, 3302−3308.
(35) Wu, Z.-S.; Shubin, Y.; Yi, S.; Khaled, P.; Xinliang, F.; Klaus, M. 3D Nitrogen-Doped Graphene Aerogel-Supported Fe_3O_4 Nanoparticles as Efficient Electrocatalysts for the Oxygen Reduction Reaction. *J. Am. Chem. Soc.* **2012**, *134*, 9082−9085.
(36) Chen, P.; Li, K. W.; Gan, W.; Min, R. G.; Jin, G.; Wen, J. Y.; Yu, H. S.; An, J. X.; Shu, H. Y. Nitrogen-doped nanoporous carbon nanosheets derived from plant biomass: an efficient catalyst for oxygen reduction reaction. *Energy Environ. Sci.* **2014**, *7*, 4095−4103.
(37) Singh, K. P.; Eun, J. B.; Jong, S. Y. Fe−P: A New Class of Electroactive Catalyst for Oxygen Reduction Reaction. *J. Am. Chem. Soc.* **2015**, *137*, 3165−3168.
(38) Liu, G.; Li, X.; Ganesan, P.; Popov, B. N. Development of non-precious metal oxygen-reduction catalysts for PEM fuel cells based on N-doped ordered porous carbon. *Appl. Catal., B* **2009**, *93*, 156−165.
(39) Zhang, L.; Wilkinson, D. P.; Liu, Y.; Zhang, J. Progress in nanostructured (Fe or Co)/N/C non-noble metal electrocatalysts for fuel cell oxygen reduction reaction. *Electrochim. Acta* **2018**, *262*, 326−336.
(40) Banham, D.; Kishimoto, T.; Sato, T.; Kobayashi, Y.; Narizuka, K.; Ozaki, J.; Zhou, Y.; Marquez, E.; Bai, K.; Ye, S. New insights into non-precious metal catalyst layer designs for proton exchange membrane fuel cells: Improving performance and stability. *J. Power Sources* **2017**, *344*, 39−45.
(41) Malko, D.; Lopes, T.; Ticianelli, E. A.; Kucernak, A. A catalyst layer optimisation approach using electrochemical impedance spectroscopy for PEM fuel cells operated with pyrolysed transition metal-N-C catalysts. *J. Power Sources* **2016**, *323*, 189−200.

https://doi.org/10.1021/acsomega.1c01036
ACS Omega 2021, 6, 20130−20138